Electrocatalysis

DOI: 10.1002/anie.201400294

Engineering Non-sintered, Metal-Terminated Tungsten Carbide Nanoparticles for Catalysis**

*Sean T. Hunt, Tarit Nimmanwudipong, and Yuriy Román-Leshkov**

Abstract: *Transition-metal carbides (TMCs) exhibit catalytic activities similar to platinum group metals (PGMs), yet TMCs are orders of magnitude more abundant and less expensive. However, current TMC synthesis methods lead to sintering, support degradation, and surface impurity deposition, ultimately precluding their wide-scale use as catalysts. A method is presented for the production of metal-terminated TMC nanoparticles in the 1–4 nm range with tunable size, composition, and crystal phase. Carbon-supported tungsten carbide (WC) and molybdenum tungsten carbide ($Mo_xW_{1-x}C$) nanoparticles are highly active and stable electrocatalysts. Specifically, activities and capacitances about 100-fold higher than commercial WC and within an order of magnitude of platinum-based catalysts are achieved for the hydrogen evolution and methanol electrooxidation reactions. This method opens an attractive avenue to replace PGMs in high energy density applications such as fuel cells and electrolyzers.*

Early transition-metal carbides (TMCs) are earth-abundant materials with established commercial use in a variety of applications owing to their favorable optical, electronic, mechanical, and chemical properties.[1–3] Tungsten carbide (WC) has garnered much attention for its catalytic similarities to the platinum group metals[4] (PGMs) in several thermo- and electrocatalytic reactions, such as biomass conversion,[2,5,6] hydrogen evolution and oxygen reduction,[7–11] and alcohol electrooxidation.[12,13] The reactivity of WC has been partially attributed to the intercalation of C to the W lattice, which gives rise to a "Pt-like" d-band electronic density states (DOS).[14] Peppernick et al. demonstrated that WC^- ions exhibit isoelectronic correspondence with Pt^- ions.[15] Because WC exhibits high thermal and electrochemical stability while resisting common catalyst poisons such as carbon monoxide and sulfur,[1–3] it has been identified as a suitable candidate to replace PGM catalysts in emerging renewable energy technologies, such as fuel cells and electrolyzers.[7–11,16–18]

[*] S. T. Hunt, T. Nimmanwudipong, Prof. Y. Román-Leshkov
Department of Chemical Engineering
Massachusetts Institute of Technology
77 Massachusetts Avenue, Cambridge, MA 02139 (USA)
E-mail: yroman@mit.edu
Homepage: http://www.romangroup.mit.edu

[**] This work was sponsored by the Chemical Sciences, Geosciences and Biosciences Division, Office of Basic Energy Sciences, Office of Science, U.S. Department of Energy, grant no. DE-FG02-12ER16352. S.T.H. thanks the National Science Foundation for financial support through the National Science Foundation Graduate Research Fellowship under Grant No. 1122374.

Supporting information for this article is available on the WWW under http://dx.doi.org/10.1002/anie.201400294.

While there are many methods to synthesize WC nanoparticles (NPs), none of the current methods can simultaneously prevent sintering of the WC nanoparticles while also mitigating surface impurity deposition. Thus, despite the promising catalytic properties of model WC surfaces, the lack of synthesis methods to produce metal-terminated WC NPs of controlled sizes has prevented its wide-spread use as an earth-abundant catalyst.[1,2,7,19] The high carburization temperatures (> ca. 700 °C) required to overcome the thermodynamic and kinetic barriers for carbon incorporation into the metal lattice induce uncontrollable particle sintering, generating particles with exceedingly low surface areas that are not suitable for commercial applications (Supporting Information, Figure S1).[1,2] Although alternative synthesis methods with unconventional heating[20–23] and carbon sources[11,17,19,24,25] have been developed to mitigate sintering, the resulting particles are extensively coked and do not feature metal-terminated surfaces. Current methods either partially mitigate sintering while generating thick surface oxide layers with excess surface carbon or fully mitigate sintering by embedding carbides within high excesses of carbon. Minute quantities of surface impurities block reactants from accessing active sites and have been shown to greatly reduce or eliminate the catalytic activity of WC.[13,26]

Consequently, catalytic studies with WC are often restricted to model materials (for example, thin films or bulk particles) where metal-terminated active sites are synthetically achievable. To date, the encouraging catalytic results obtained with these model materials have not been translated to analogous metal-terminated nanoscale formulations. For instance, surface science studies have shown that planar, metal-terminated polycrystalline α-WC foils are more active than comparable planar Pt foils for anodic methanol electrooxidation (MOR),[12,13] but W_2C microparticles and α-WC nanowires containing synthesis-inherent surface carbon impurities are inactive towards MOR.[27,28] Accordingly, the unique electrocatalytic properties arising from high degrees of coordinative unsaturation and quantum size effects for WC NPs continue to be known only theoretically[29] and remain experimentally unexplored. To bridge this "materials gap" and translate the promising surface science studies for replacing PGMs with WC in commercial devices, it is critical to develop new synthetic methods capable of generating non-sintered, metal-terminated TMC NPs.[2,7]

Herein, we demonstrate a method to produce mono- and multimetallic TMC NPs with tunable size, composition, and crystal phase. This synthesis method is versatile, allowing the deposition of well-dispersed, metal-terminated TMC NPs in the range of 1–4 nm on a high-surface-area support with loadings exceeding 40 wt %. The three-step process is

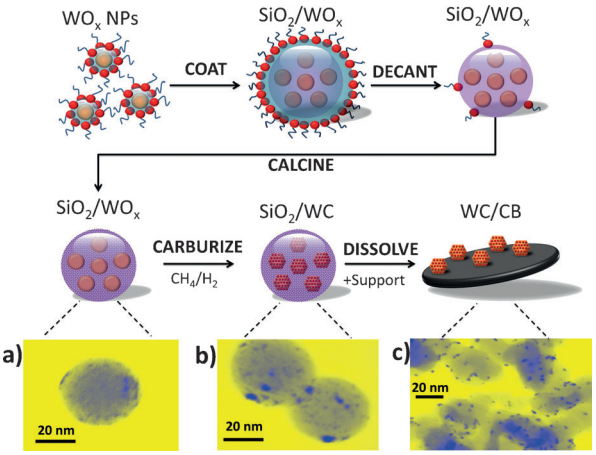

Figure 1. Representation of the removable ceramic coating method for the synthesis of WC/CB. a) STEM image of silica-encapsulated tungsten oxide NPs. b) STEM image of silica-encapsulated WC NPs. c) STEM image of WC NPs supported on carbon black.

depicted in Figure 1. First, a reverse microemulsion (RME) is used to create transition-metal oxide NPs encapsulated within silica (SiO_2) nanospheres. The resulting composite particles are subjected to a high-temperature carburization process, wherein the SiO_2 coating serves as a hard template to prevent NP sintering while allowing the diffusion of carburization gases onto the metal oxide surfaces (Figure 1 b). Next, a liquid dispersion of naked TMC NPs is obtained by dissolving the SiO_2 shell, and supported NPs are obtained by mixing a high-surface-area solid with the dispersion (Figure 1 c). The method is general, being applicable to virtually any metal oxide formulation that can be transformed into a carbide. We exemplify the method herein through the synthesis of monometallic tungsten carbide (WC) and bimetallic molybdenum tungsten carbide ($Mo_xW_{1-x}C$) NPs. Using hydrogen evolution (HER) and methanol electrooxidation (MOR) as probe reactions, we show that these TMC NPs supported on Vulcan XC-72r carbon black (CB) are highly stable and attain capacitances and catalytic activities that are orders of magnitude higher than those obtainable with analogous carbides synthesized with current methods, approaching the activities of PGM-based electrocatalysts. To the best of our knowledge, this is the first method capable of generating metal-terminated WC-based nanoparticles of less than 5 nm that are active for both HER and MOR.

An RME, wherein nanosized water domains are dispersed in non-polar media by a nonionic surfactant at room temperature, is a versatile solution-based method to tune the size and composition of mono- and heterometallic metal oxide NPs.[30–32] In a single step, about 100 ultrasmall (1–2 nm) WO_x NPs were encased within circa 40 nm silica nanospheres (Figure 1 a) at metal loadings of about 20 wt% when using a nonionic Brij-L4/*n*-heptane/water RME system (Supporting Information, Figures S3–S7 and S9–S18). High-angle annular dark field scanning transmission electron microscopy (STEM) images show that controlled temperature treatments of the encapsulated WO_x NPs with sequential oxidizing (air, 450 °C), reducing (21 % CH_4/H_2 mixture, 590 °C), and carburizing (21 % CH_4/H_2 mixture, 835 °C) conditions result in the formation of carbide NPs in the 1–4 nm range (Figure 1 b). An H_2 treatment at 835 °C followed by exposure to 1 % O_2/N_2 at 25 °C scavenges residual surface carbon and forms a surface-passivating oxide layer that allows handling in ambient conditions.[9,16] We hypothesize that the heat treatment promotes the formation of micropores on the silica shell, allowing H_2 and CH_4 to reach the surface of the oxide, while diminishing particle migration and coalescence (Supporting Information, Figure S7). This phenomenon is consistent with recent reports showing that sintering reduction during high temperature catalytic reactions (up to about 750 °C) is achieved by coating noble metals with microporous and mesoporous ceramic overlayers.[33–35] Measured particle-size distributions (PSD, Figure 2 c) indicate that sintering is largely mitigated within these silica nanospheres even after prolonged exposure to carburizing conditions at 835 °C and as high as 950 °C (Supporting Information, Figures S5, S10, S11). The slight increase in PSD after carburization is attributed to the lateral diffusion of surface-bound NPs on the silica nanospheres.

The PSD, crystal phase, and composition of TMC NPs can be tuned by altering synthesis parameters. Powder X-ray diffractograms (PXRD) diffractograms shown in Figure 2 a confirm the presence of phase-pure face-centered cubic (fcc) WC particles (β-WC or WC_{1-x}) when using standard RME and heat treatment procedures (see above). Increasing the size of silica nanospheres from 40 to 50 nm resulted in a decrease in the PSD of WC NPs from 1–3 nm to 1–2 nm (Figure 2 b). Lowering the carburization temperature to 775 °C and decreasing the CH_4/H_2 ratio to 18 % resulted in the formation of phase-pure tungsten semicarbide (W_2C) NPs (Figure 2 a). While β-WC is typically considered a high-temperature phase,[36] both β-WC and the traditional hexagonal phase (α-WC) were synthesized under identical carburization conditions (835 °C, 21 % CH_4/H_2). α-WC was obtained when lowering the methanol/heptane ratio used for precipitation prior to carburization (Figure 2 a). The resulting α-WC NPs were larger (3–6 nm) than the β-WC NPs and featured quartz-like domains within the silica spheres (Figure 2 a,c). Although no experimental methods had been reported before for the synthesis of β-WC NPs in the 1–4 nm range, recent density functional theory (DFT) studies have predicted that both the fcc β-WC lattice and the hexagonal α-WC lattice are stable phases for NPs of this size.[29]

Combining metal precursors at the RME stage allows the synthesis of heterometallic "double" carbide NPs with a high degree of compositional control. In this respect, $Mo_xW_{1-x}O_y$ NPs were synthesized by mixing tungsten and molybdenum precursors (Supporting Information, Figures S2–S4, S14–S17). These heterometallic oxides were subjected to similar encapsulation and carburization procedures as those used for monometallic carbides to generate double carbides either in a β-WC phase (Figure 2 a) or in an α-WC phase (Supporting Information, Figure S17). A separate molybdenum carbide (Mo_2C) phase was not observed, which is consistent with reports showing the formation of double carbide microparticles.[37] STEM with energy-dispersive X-ray spectroscopy

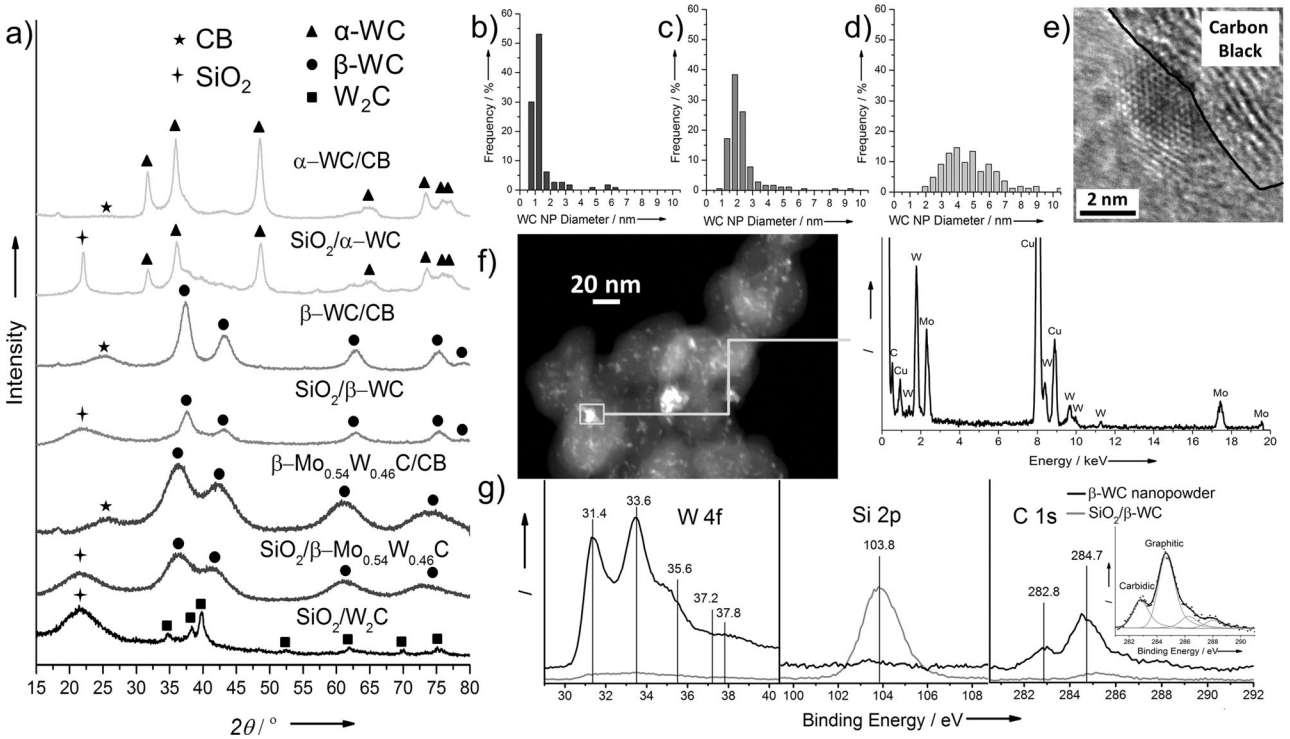

Figure 2. Material characterization. a) PXRD diffractograms (in ascending order) of silica-coated and CB-supported W_2C, β-$Mo_{0.54}W_{0.46}C$, β-WC, and α-WC. b) PSD for β-WC tuned for 1 nm NPs. c) PSD for 1–3 nm β-WC tuned for 2 nm NPs. d) PSD for 3-6 nm α-WC. e) HR-TEM image of a 2 nm β-WC NP. f) STEM image of a 25 wt% β-$Mo_{0.54}W_{0.46}C$/CB and the corresponding EDX spectra for a single NP showing the presence of both W and Mo (the presence of the Cu background arises from the TEM grid material). g) XPS spectra of SiO_2/β-WC and the β-WC nanopowder obtained post-ABF-dissolution for W, Si, and C signals.

(EDX) analysis confirmed the presence of both W and Mo within single NPs (Figure 2 f; Supporting Information, Figure S20). The exact compositions were determined using inductively coupled plasma (ICP) analysis. The compositions synthesized range from $Mo_{0.02}W_{0.98}C$ to $Mo_{0.54}W_{0.46}C$ (Supporting Information, Figure S20).

Silica and other hard template materials are electrically insulating; therefore, the resulting composite materials are not amenable for electrocatalysis. For this reason, synthesis methods using hard templates, such as SBA-15,[38] have not been geared towards producing electrocatalytically active WC. Moreover, such hard templating methods suffer from being synthetically complex, having low metal loadings, and lacking control over crystal phase and particle size. Critical to our method, we show that the silica shell can be fully removed under acidic (20 wt% ammonium bifluoride (ABF)) or alkaline (0.5 M NaOH) conditions to yield solutions containing dispersed, non-sintered naked carbide NPs (Supporting Information, Figure S19). Although WC dissolves in strong alkaline media,[39] PXRD diffractograms show that both α-WC, β-WC, and β-$Mo_{0.54}W_{0.46}C$ are stable in ABF (Figure 2 a,f). Notably, re-dispersing α- and β-WC NPs in water or ethanol showed no signs of sedimentation after 20 days (Supporting Information, Figure S19). In contrast with other methods,[40] neither sonication nor polymeric agents are required to disperse the WC NPs. Targeted loadings (even in excess of 40 wt%) are obtained simply by mixing specific amounts of CB directly with the SiO2/WC/ABF solution or the waterborne dispersion. STEM images confirm that highly dispersed TMC NPs on CB are obtained following this procedure (Figure 1 c, 2 f; Supporting Information, Figure S12). Decoupling carburization from support deposition is important because it allows dispersing the TMC NPs on a variety of supports, including those that would be damaged during the harsh carburization conditions.

X-ray photoelectron spectroscopy (XPS) analyses on passivated β-WC nanopowders post ABF-dissolution revealed that the carbide NP surfaces are free of impurities, with undetectable quantities of Si, minimal graphitic surface carbon, and indiscernible bulk oxidation formation (Figure 2 g). Specifically, strong W 4f signals are found at 31.4 and 33.6 eV, which correspond to reduced metallic W. The small peaks at 36.2 and 38.3 eV correspond to WO_x in a surface passivating layer. These surface oxides can be easily removed prior to catalytic testing by in situ treatment in H_2 or by quick alkaline rinses without impacting the bulk carbide structure.[1,9,16,39] A carbidic C 1s signal at 282.8 eV indicates that the NP surfaces are carbide-terminated and that surface graphitic impurities are largely mitigated (Figure 2 g). The locations and relative intensities are in agreement with previous literature for pristine WC thin films.[13,16] High-resolution TEM images confirm that graphitic carbon is not present in detectable amounts on the surface of the NPs (Figure 2 e; Supporting Information, Figure S13). In contrast, reported TEM characterization data for conventional TMC synthesis methods show extensive surface carbon overlayers

surrounding each nanoparticle, which obfuscate the carbidic C 1s signal.[11,17,19,24]

HER is a well-established probe reaction for comparing WC materials. HER electrocatalytic activities of α-WC/CB and β-$Mo_{0.06}W_{0.94}C$/CB materials were compared to conventional WC catalysts (using commercial WC microparticles and NPs synthesized using the "urea glass" method)[19] and commercial 40 wt% Pt/CB. All working electrodes were loaded with 50 μg of catalyst by total weight and subjected to capacitance measurements in 0.5 M H_2SO_4 (see the Supporting Information, Table S1 for N_2 adsorption isotherms). The capacitances of the supported β-carbides were similar to Pt/CB and over 1.6 orders of magnitude higher than bare CB or the carbide controls (Supporting Information, Figures S23, S24). These data indicate that 40 wt% WC/CB and 40 wt% Pt/CB with equivalent masses and geometric surface areas have similar electroactive surface areas, and they also suggest that supported β-carbides can serve as high power density supercapacitors with similar capacitances as supported amorphous RuO_2 nanoparticles prepared using a standard method (Supporting Information, Figures S25, S26).[41]

Linear sweep voltammograms (LSVs) for each material under HER conditions show that TMC NPs synthesized with our method are highly stable and easily regenerated, achieving substantially higher HER currents at lower overpotentials when compared to the commercial or the "urea glass" WC (Figure 3a). We note that the large slope of the 40% Pt/CB control catalyst can be attributed its high loading and the low pH of the electrolyte, while its offset from 0 V vs. RHE can be attributed to the use of a static working electrode (Supporting Information, Figure S27).[42] Chronoamperometry (CA) and chronopotentiometry (CP) measurements (Table 1) show that

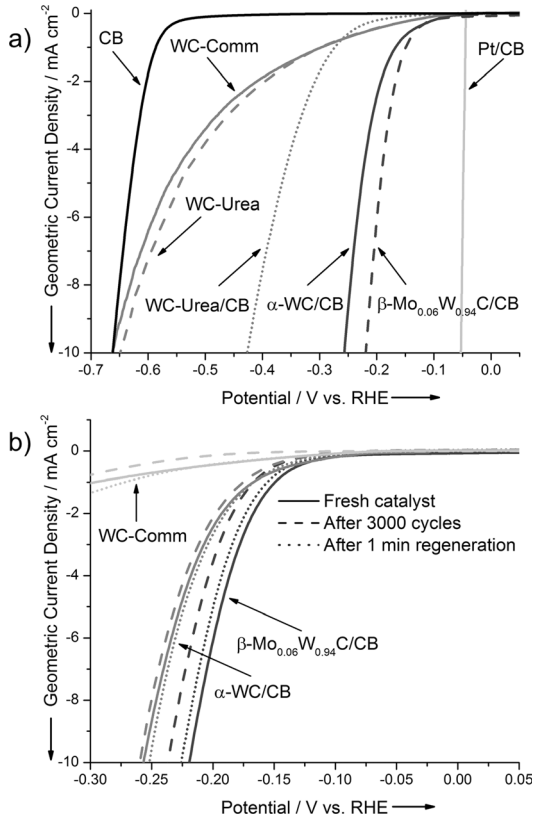

Figure 3. HER activity, stability, and catalyst Regeneration. a) Initial HER LSVs at 2 mV s^{-1} in H_2-saturated 0.5 M H_2SO_4 at RT. b) LSVs at 2 mV s^{-1} in H_2-saturated 0.5 M H_2SO_4 at RT showing initial HER activity, the final activity after 3000 cycles between −0.3 and +0.6 V vs. RHE at a scan rate of 50 mV s^{-1}, and the regenerated activity after dipping the spent electrodes in 0.1 M NaOH for one minute. All of the CB-supported catalysts are loaded at 40 wt%.

Table 1: HER activity, stability, and regeneration comparison.

Catalyst[a]	Initial j[b] $j_{\eta=290mV}$* [mA cm^{-2}]	Initial η[c] η_i @ $j_{Cat=1}$ [mV]	Final η[d] η_f @ $j_{Cat=1}$ [mV]	Regenerated η[e] η_r @ $j_{Cat=1}$ [mV]
Pt/CB	−150	44	44	–
β-$Mo_{0.06}W_{0.94}C$/CB	−27	156	166	161
α-WC/CB	−21	165	175	165
Commercial WC	−1.0	290	311	281
WC-Urea/CB	−1.3	280	–	–
WC-Urea	−1.1	270	–	–
Vulcan CB	−0.1	360	–	–

[a] All of the CB-supported catalysts are loaded at 40 wt%. [b] Initial cathodic current density at a fixed overpotential of $\eta = 290$ mV vs. RHE. [c] Initial overpotential at 1 mA cm^{-2} of cathodic current. [d] Overpotential at 1 mA cm^{-2} after 3000 cycles between −0.3 and +0.6 V vs. RHE. [e] Overpotential at 1 mA cm^{-2} after regeneration of the spent working electrode after it was dipped in 0.1 M NaOH solution for one minute.

α-WC/CB and β-$Mo_{0.06}W_{0.94}C$/CB exhibit current densities that are 1.4 orders of magnitude higher than either of the carbide controls. To drive 1 mA cm^{-2} of cathodic current, α-WC/CB and β-$Mo_{0.06}W_{0.94}C$/CB required an overpotential that was lower by more than 100 mV than either of the carbide controls (Table 1). While Mo_2C/CB and MoS_2 have been shown to be active HER electrocatalysts,[43,44] we demonstrate the superior stability of both the CB-supported α and β-carbide NPs as well as a facile electrode regeneration method. After 3000 cycles between −0.3 V and +0.6 V vs. RHE, both the α and β carbides exhibited minimal deactivation (Figure 3b), showing an increase in overpotential of about 10 mV to drive 1 mA cm^{-2} (Table 1). Notably, the catalysts can be easily regenerated by dipping the electrode for 1 min in a 0.1 M aqueous NaOH solution to remove surface oxides (Figure 3b, Table 1).

PXRD diffractograms of the spent and subsequently regenerated catalysts indicate that both the α and β-carbides are stable after 3000 cycles (Supporting Information, Figure S28). Intrinsically, WC has a stronger hydrogen binding energy than Pt, which translates to a higher onset potential of HER.[9,16] This inherent thermodynamic limitation is largely offset by the substantially lower cost and higher abundance of WC in comparison to PGMs,[7] as well as its higher activity, stability, conductivity, and ease of regeneration in comparison to other earth-abundant alternatives. We attribute the higher activity of the bimetallic β-$Mo_{0.06}W_{0.94}C$ relative to α-WC to its smaller PSD (Figure 2c), its higher surface area (Supporting Information, Table S1), as well as a bimetallic effect. Thin-film studies have shown that pristine Mo_2C is more active towards HER than pristine WC,[8] but Mo_2C features lower

electrochemical stability than WC.[45] A bimetallic $Mo_xW_{1-x}C$ allows us to achieve a compromise between the activity of Mo_2C and the stability of WC in a single material. Insertion of Mo heteroatoms compresses the WC lattice owing to the larger Wigner–Seitz radius of Mo, potentially giving rise to new catalytic activities by modulation of the d-band surface electronic density of states (DOS).

Unlike other earth-abundant materials, WC is unique in its "Pt-like" ability to catalyze a broad array of important thermal and electrochemical reactions. However, activating WC for more complex reactions such as MOR requires pristine metal-terminated surfaces that are free from surface carbon or thick oxide layers.[13] Thus, MOR activity serves as a probe to test if the WC nanoparticles are metal-terminated and free of surface impurities. For the first time, we show that CB-supported α-WC NPs are highly active and stable electrocatalysts for MOR, with power densities approaching those of commercial Pt-based materials (Supporting Information, Figures S29 to S36). Figure 4 shows CA responses under MOR conditions, wherein a strong oxidizing potential

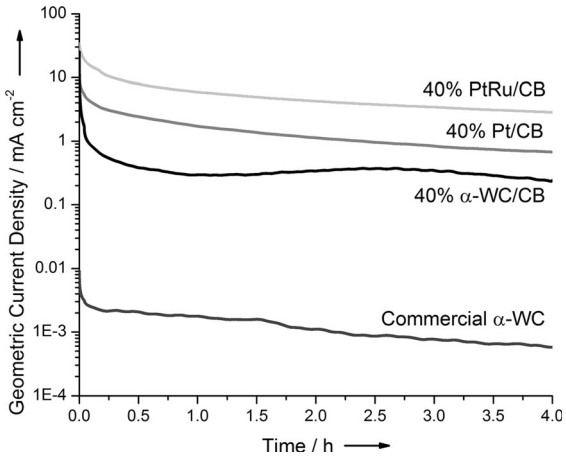

Figure 4. MOR electrochemical activity comparison. Chronoamperometric responses in Ar-saturated 0.5 M H_2SO_4 and 2.0 M CH_3OH at 40 °C held potentiostatically at +0.75 V vs. RHE over 4 h.

of +0.75 V was chosen to verify that the measured currents were catalytic in nature, as reported in prior studies,[27,28] and to highlight the remarkable long-term stability of the carbide NPs under harsh conditions. After 4 h, 40 wt % α-WC/CB was over 2.5 orders of magnitude more active than a commercial α-WC catalyst. Over the last 15 min of the 4 h experiments, the commercial WC drove an average current density of $0.58 \pm 0.01\ \mu A\,cm^{-2}$, while α-WC/CB drove $235 \pm 8\ \mu A\,cm^{-2}$. The "urea glass" WC was inactive, which is most likely due to excessive surface carbon deposition during synthesis. We attribute the slight activity of commercial WC from exposed metal-terminated sites achieved during the top-down ball-milling synthesis process. Remarkably, the activity of the α-WC/CB material was about 33 % of that measured for a commercial 40 wt % Pt/CB catalyst ($696 \pm 6\ \mu A\,cm^{-2}$), and approximately one order of magnitude less active than a bifunctional 40 wt % PtRu/CB ($2{,}850 \pm 15\ \mu A\,cm^{-2}$). Further activity and stability improvements can now be achieved through alloying and/or surface admetal decoration as suggested by surface science studies.[7,12] In Figure 4, integration of the charge under the CA response for the 40 wt % α-WC/CB catalyst indicates that the current is catalytic and cannot be attributed to capacitive discharging or bulk oxidation of WC to WO_3 (Supporting Information, Figure S35). Specifically, after 4 h at +0.75 V in 0.5 M H_2SO_4 at 40 °C without methanol, the average final current for α-WC/CB was $6.0 \pm 1.7\ \mu A\,cm^{-2}$ or 2.5 % of the current density achieved in the presence of methanol.

In summary, this "removable ceramic coating method" is a versatile technique to synthesize non-sintered, ultrasmall, metal-terminated monometallic and heterometallic TMCs with strict control over composition, crystal phase, and PSD. The resulting NPs can be stored as a nanodispersion or deposited at any desired loading onto a high-surface-area support material. Importantly, this method is general and could be extended to synthesize not only other monometallic and heterometallic carbides, but also a variety of transition-metal nitrides and phosphides by replacing methane with the corresponding reactive precursor. We envision that metal-terminated TMC NPs will open interesting avenues for synthesizing advanced TMC-PGM core–shell NPs that could substantially reduce noble metal loadings in catalysts using PGMs.[7,16] While the PGMs are too scarce and expensive to support a global renewable energy economy,[46] we demonstrate that earth-abundant TMCs engineered with finely controlled sizes and surfaces can achieve the required energy densities and stabilities for use in a variety of burgeoning renewable energy platforms.

Experimental Section

Detailed procedures for the synthesis of the catalysts as well as characterization and reactivity data are provided in the Supporting Information. Electrochemical measurements were performed in a three-electrode cell using a CHI 627E potentiostat equipped with an Ag/AgCl (in 1 M KCl) reference electrode and a Pt wire counter electrode. Catalyst inks were prepared by sonicating 7.5 mg of catalyst (by total mass) in 1 mL of degassed ultrapure water and 20 μL of 5 % Nafion 117 solution. 7 μL of ink were dropped onto a freshly polished (using 0.05 μm alumina powder) 0.071 cm^2 glassy carbon disk electrode and dried under vacuum. Separate disk electrodes were used for PGM-containing and carbide-containing materials.

Received: January 10, 2014
Published online: April 2, 2014

Keywords: carbides · electrocatalysis · hydrogen evolution reaction · nanoparticles · sinter resistance

[1] S. T. Oyama, *The Chemistry of Transition Metal Carbides and Nitrides*, Blackie, Glasgow, **1996**.
[2] A. L. Stottlemyer, T. G. Kelly, Q. Meng, J. G. Chen, *Surf. Sci. Rep.* **2012**, *67*, 201 – 232.
[3] J. G. Chen, *Chem. Rev.* **1996**, *96*, 1477 – 1498.
[4] R. B. Levy, M. Boudart, *Science* **1973**, *181*, 547 – 549.
[5] N. Ji, T. Zhang, M. Zheng, A. Wang, H. Wang, X. Wang, J. G. Chen, *Angew. Chem.* **2008**, *120*, 8638 – 8641; *Angew. Chem. Int. Ed.* **2008**, *47*, 8510 – 8513.

[6] R. W. Gosselink, D. R. Stellwagen, J. H. Bitter, *Angew. Chem.* **2013**, *125*, 5193 – 5196; *Angew. Chem. Int. Ed.* **2013**, *52*, 5089 – 5092.
[7] D. V. Esposito, J. G. Chen, *Energy Environ. Sci.* **2011**, *4*, 3900 – 3912.
[8] T. G. Kelly, S. T. Hunt, D. V. Esposito, J. G. Chen, *Int. J. Hydrogen Energy* **2013**, *38*, 5638 – 5644.
[9] D. V. Esposito, S. T. Hunt, A. L. Stottlemyer, K. D. Dobson, B. E. McCandless, R. W. Birkmire, J. G. Chen, *Angew. Chem.* **2010**, *122*, 10055 – 10058; *Angew. Chem. Int. Ed.* **2010**, *49*, 9859 – 9862.
[10] X. Zhou, Y. Qiu, J. Yu, J. Yin, S. Gao, *Int. J. Hydrogen Energy* **2011**, *36*, 7398 – 7404.
[11] A. T. Garcia-Esparza, D. Cha, Y. Ou, J. Kubota, K. Domen, K. Takanabe, *ChemSusChem* **2013**, *6*, 168 – 181.
[12] E. C. Weigert, A. L. Stottlemyer, M. B. Zellner, J. G. Chen, *J. Phys. Chem. C* **2007**, *111*, 14617 – 14620.
[13] X. Yang, Y. C. Kimmel, J. Fu, B. E. Koel, J. G. Chen, *ACS Catal.* **2012**, *2*, 765 – 769.
[14] L. H. Bennett, J. R. Cuthill, A. J. McAlister, N. E. Erickson, R. E. Watson, *Science* **1974**, *184*, 563 – 565.
[15] S. J. Peppernick, K. D. D. Gunaratne, A. W. Castleman, Jr., *Proc. Natl. Acad. Sci. USA* **2010**, *107*, 975 – 980.
[16] D. V. Esposito, S. T. Hunt, Y. C. Kimmel, J. G. Chen, *J. Am. Chem. Soc.* **2012**, *134*, 3025 – 3033.
[17] Z. Yan, M. Cai, P. K. Shen, *Sci. Rep.* **2013**, *50*, 1646 – 1653.
[18] M. Wu, X. Lin, A. Hagfeldt, T. Ma, *Angew. Chem.* **2011**, *123*, 3582 – 3586; *Angew. Chem. Int. Ed.* **2011**, *50*, 3520 – 3524.
[19] C. Giordano, C. Erpen, W. Yao, M. Antonietti, *Nano Lett.* **2008**, *8*, 4659 – 4663.
[20] S. R. Vallance, H. J. Kitchen, C. Ritter, S. Kingman, G. Dimitrakis, D. H. Gregory, *Green Chem.* **2012**, *14*, 2184 – 2192.
[21] P. K. Shen, S. Yin, Z. Li, C. Chen, *Electrochim. Acta* **2010**, *55*, 7969 – 7974.
[22] A. V. Nikiforov, I. M. Petrushina, E. Christensen, N. V. Alexeev, A. V. Samokhin, N. J. Bjerrum, *Int. J. Hydrogen Energy* **2012**, *37*, 18591 – 18597.
[23] Z. Z. Fang, X. Wang, T. Ryu, K. S. Hwang, H. Y. Sohn, *Int. J. Refract. Met. Hard Mater.* **2009**, *27*, 288 – 299.
[24] Z. Abdullaeva, E. Omurzak, C. Iwamoto, H. Okudera, M. Koinuma, S. Takebe, S. Sulaimankulova, T. Mashimo, *R. Soc. Chem. Adv.* **2013**, *3*, 513 – 519.
[25] J. A. Nelson, M. J. Wagner, *Chem. Mater.* **2002**, *1*, 1639 – 1642.
[26] Y. C. Kimmel, D. V. Esposito, R. W. Birkmire, J. G. Chen, *Int. J. Hydrogen Energy* **2012**, *37*, 3019 – 3024.
[27] R. Ganesan, J. S. Lee, *Angew. Chem.* **2005**, *117*, 6715 – 6718; *Angew. Chem. Int. Ed.* **2005**, *44*, 6557 – 6560.
[28] Y. Yan, L. Zhang, X. Qi, H. Song, J.-Y. Wang, H. Zhang, X. Wang, *Small* **2012**, *8*, 3350 – 3356.
[29] V. G. Zavodinsky, *Int. J. Refract. Met. Hard Mater.* **2010**, *28*, 446 – 450.
[30] L. Xiong, T. He, *Chem. Mater.* **2006**, *18*, 2211 – 2218.
[31] K. Panda, S. P. Moulik, B. B. Bhowmik, R. Das, *J. Colloid Interface Sci.* **2001**, *235*, 218 – 226.
[32] A. Zarur, J. Ying, *Nature* **2000**, *403*, 65 – 67.
[33] J. Lu, B. Fu, M. C. Kung, G. Xiao, J. W. Elam, H. H. Kung, P. C. Stair, *Science* **2012**, *335*, 1205 – 1208.
[34] Y. Dai, B. Lim, Y. Yang, C. M. Cobley, W. Li, E. C. Cho, B. Grayson, P. T. Fanson, C. T. Campbell, Y. Sun, et al., *Angew. Chem.* **2010**, *122*, 8341 – 8344; *Angew. Chem. Int. Ed.* **2010**, *49*, 8165 – 8168.
[35] S. H. Joo, J. Y. Park, C.-K. Tsung, Y. Yamada, P. Yang, G. A. Somorjai, *Nat. Mater.* **2009**, *8*, 126 – 131.
[36] H. Tulhoff, H. C. S. Berlin, W. Goslar, *Ullman's Encycl. Ind. Chem.* **2012**, 565 – 582.
[37] G. Kawamura, *J. Electrochem. Soc.* **1987**, *134*, 1653 – 1658.
[38] L. Hu, S. Ji, T. Xiao, C. Guo, P. Wu, P. Nie, *J. Phys. Chem. B* **2007**, *111*, 3599 – 3608.
[39] M. C. Weidman, D. V. Esposito, I. J. Hsu, J. G. Chen, *J. Electrochem. Soc.* **2010**, *157*, F179.
[40] C. Giordano, W. Yang, A. Lindemann, R. Crombez, J. Texter, *Colloids Surf. A* **2011**, *374*, 84 – 87.
[41] H. Kim, B. N. Popov, *J. Power Sources* **2002**, *104*, 52 – 61.
[42] T. J. Schmidt, H. A. Gasteiger, G. D. Stab, P. M. Urban, D. M. Kolb, R. J. Behm, *J. Electrochem. Soc.* **1998**, *145*, 2354 – 2358.
[43] W.-F. Chen, C.-H. Wang, K. Sasaki, N. Marinkovic, W. Xu, J. T. Muckerman, Y. Zhu, R. R. Adzic, *Energy Environ. Sci.* **2013**, *6*, 943 – 951.
[44] J. Kibsgaard, Z. Chen, B. N. Reinecke, T. F. Jaramillo, *Nat. Mater.* **2012**, *11*, 963 – 969.
[45] M. C. Weidman, D. V. Esposito, Y.-C. Hsu, J. G. Chen, *J. Power Sources* **2012**, *202*, 11 – 17.
[46] R. B. Gordon, M. Bertram, T. E. Graedel, *Proc. Natl. Acad. Sci. USA* **2006**, *103*, 1209 – 1214.

